

IMECE2006-16190

CONTROL OF MEMS NANOPositionERS WITH NANO-SCALE RESOLUTION

Jason J. Gorman*, **Yong-Sik Kim**, and **Nicholas G. Dagalakis**
Intelligent Systems Division
National Institute of Standards and Technology
Gaithersburg, Maryland 20899-8230
*contact author: gorman@nist.gov

ABSTRACT

Several approaches for the precision control of micro-scale positioning mechanisms, or MEMS nanopositioners, are presented along with initial experimental results which demonstrate nano-scale positioning resolution. The MEMS nanopositioners discussed in this paper are novel precision mechanisms comprised of a bent-beam thermal actuator and a flexure mechanism for each degree of freedom (DOF). These mechanisms can be used for a host of ultra-precision positioning applications, including nanomanipulation, scanning probe microscopy, high-density data storage and beam steering arrays. Concentrating on a 1 DOF MEMS nanopositioner, empirical static and dynamic models have been derived using characterization data obtained from experiments with optical and laser probe microscopes. Based on these models, three control approaches have been developed: 1) a quasi-static nonlinear open-loop controller, 2) a nonlinear forward compensator, and 3) a nonlinear PI controller. Simulation and initial experimental results are presented, and the benefits of each of these approaches are discussed.

INTRODUCTION

The utilization of microelectromechanical systems (MEMS) for nanotechnology research and nanomanufacturing has a number of critical applications. Micro-scale scanning probe microscopes are one particular system, such as the mechanism developed by Xu et al. [1], among others. More exotic systems include the high density data storage system using active microcantilever arrays presented by Eleftheriou et al. [2] and the micro-scale atomic trapping instrument developed by Gollasch et al. [3]. The combination of MEMS and nanotechnology presents a number of new challenges not experienced in more common MEMS applications in sensors

and telecommunications. Most importantly, precision motion control of MEMS actuators is critical, where resolution, accuracy and repeatability are expected to be on the order of nanometers. In this paper, we present results on the precision control of MEMS nanopositioning mechanisms which may further the utilization of MEMS in nanotechnology.

In recent years, there have been some efforts to demonstrate motion capabilities of MEMS at the nano-scale. Horsley et al. [4] have presented an electrostatic actuator capable of performing 100 nm steps at high bandwidth. Hoens et al. [5] have demonstrated nanometer steps with an electrostatically actuated dipole surface drive. A thermal actuator was presented by Hubbard and Howell [6] that can perform motion steps on the order of 100 nm. However, closed-loop control was only used in [4], even though closed-loop tracking is particularly important for micro-scale scanning probe microscopes and nanomanipulators.

In this paper, we present results on the precision motion control of a one degree of freedom (DOF) MEMS nanopositioner, which is composed of a bent-beam thermal actuator and a flexure mechanism for amplifying and guiding the actuator motion. Three independent control approaches have been studied: 1) quasi-static nonlinear open-loop control, 2) nonlinear feedforward compensation, and 3) nonlinear PI control. First, a description of the MEMS nanopositioner is presented, along with a discussion of the characterization tools used. Then, static and dynamic experimental results are presented and an empirical dynamic model of the mechanism is discussed. Based on this model, the three controller designs are described and simulation results are presented to compare the benefits and drawbacks of each of the approaches. Initial experimental results for the nonlinear open-loop controller are also presented and discussed.

SYSTEM DESCRIPTION

In this section, the micro-scale nanopositioning mechanism, or MEMS nanopositioner, will be described. The instrument used to measure the motion of the mechanism, the laser reflectance microscope, will also be presented.

MEMS Nanopositioner

The MEMS nanopositioner focused on in this paper is a 1 DOF mechanism shown in Fig. 1. A bent-beam thermal actuator is used to drive the input of a parallel dual-lever flexure mechanism. This flexure mechanism is designed to amplify the motion of the actuator while also guaranteeing that the motion remains straight along the axis of motion of the actuator. The motion range of this mechanism is approximately 28 μm , although it is typically driven within a smaller range. The input voltage range is 0 V to approximately 18 V. A more detailed description of this mechanism is presented in [7].

This mechanism is particularly good for nanopositioning because the flexure mechanism has very low cross-talk between the X and Y axes, and the rotational errors of the stage are extremely small. In order to utilize this mechanism to the fullest extent, a precision control system is required to achieve nano-scale positioning resolution, which is the focus of this paper.

Laser Reflectance Microscope

Embedding position sensors, typically either capacitance or piezoresistive, inside MEMS is common practice for precision devices. However, for these sensors to operate effectively, instrumentation for calibrating the sensors is necessary. For in-plane motion, optical microscopy, scanning electron microscopy (SEM), and white light interferometry are commonly used. With the exception of the SEM, these instruments have resolutions on the order of hundreds of nanometers. Although the SEM is an excellent tool for MEMS metrology, the performance variations between operation in air versus the vacuum chamber of an SEM cause difficulties in accurate calibration. Therefore, an instrument that can measure in-plane motion with resolution on the order of nanometers and can operate in air is desirable. The laser reflectance microscope utilized by Hickey et al. [8] for time and frequency measurements of thermal actuators is an attractive solution. We have adapted this approach to achieve position measurements with nanometer resolution for characterizing the MEMS nanopositioner.

Laser reflectance microscopy is a simple concept but requires significant tuning to achieve precision position measurements. In its simplest form, a laser is focused to a point using a microscope objective. The focal point of the laser is positioned on a moving edge of the MEMS such that a portion of the beam is reflected back through the objective. As the MEMS moves, the percentage of beam reflected will change. By measuring the intensity of the reflection and the position of MEMS with an optical microscope, the instrument can be calibrated.

The configuration of the laser reflectance microscope (LRM) used in the experiments presented in this paper is described by Fig. 2. A fiber-coupled laser with a wavelength of 635 nm and a maximum power of 3.18 mW is collimated using

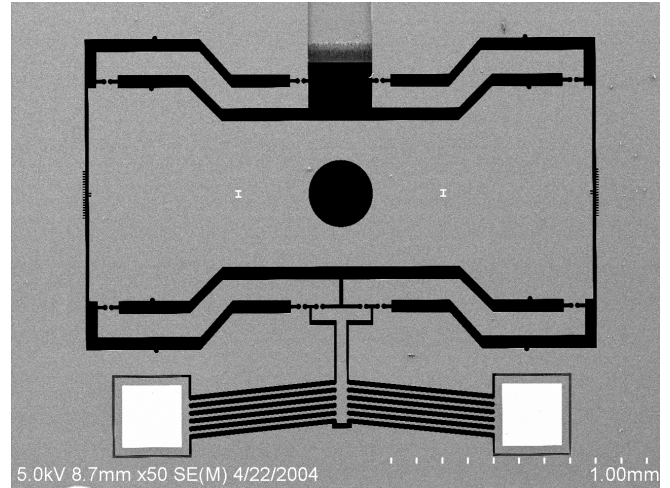


Fig. 1 One DOF MEMS nanopositioner (SEM image)

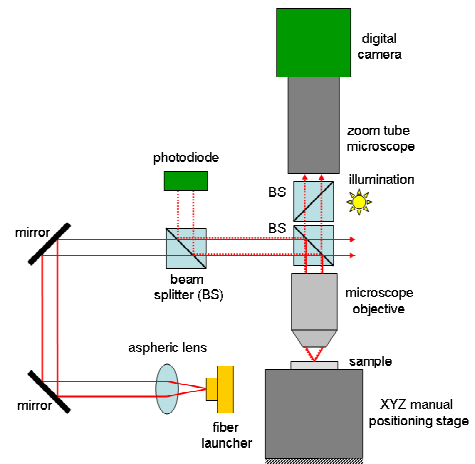


Fig. 2 Laser reflectance microscope

an aspheric lens. The beam (solid red lines) is then directed by two broadband mirrors through a 50/50 beam splitter. Half of the beam power continues into a second beam splitter, where the beam is halved again. The reflected portion of the beam goes through the back aperture of a 50X microscope objective and is focused onto the surface of the MEMS under test. A portion of the beam (dashed red lines) is then reflected back through the microscope objective, split in half by one beam splitter and then again by a second. The reflection off of the second beam splitter is directed into a photodiode where the reflection intensity is measured. Only critical beam paths are shown in Fig. 2 to avoid confusion.

The LRM also works as a standard optical microscope so that the position of the MEMS can be captured using a digital camera while measuring the reflection intensity with the photodiode. The calibration procedure will be described in the next section. This approach has a number of benefits for measuring MEMS motion at the nano-scale. First, since this is an optical technique utilizing high-bandwidth photodiodes, the

sensing bandwidth is also extremely high (~90 kHz or greater). Second, the position resolution is a function of the laser power, laser focal spot size, and photodiode noise. By increasing the laser power and minimizing the spot size, the resolution can go below 1 nm. However, depending on the application one may wish to have coarser resolution but a larger measurement range, which can also be achieved by adjusting the spot size. As will be discussed later, the main drawback of this approach is the resulting nonlinear function between the displacement and reflection intensity. In the following section static and dynamic characterization results for the MEMS nanopositioner obtained using the LRM will be presented.

EXPERIMENTAL CHARACTERIZATION

In this section, results from the characterization experiments for the static and dynamic behavior of the MEMS nanopositioner are presented. A number of proposed models for thermal actuators have been described in the literature. However, due to geometric and material parameter variations, the best approach for designing a model-based controller is to use an empirical model. As will be shown shortly, the relationship between the input voltage and the resulting displacement for thermal actuators is nonlinear. In order to capture the complete behavior of the mechanism, a static characterization is used to measure this nonlinear relationship while a swept-sine frequency measurement provides the dynamic behavior.

Static Characterization

The relationship between the input voltage and resulting displacement was measured by applying a series of static voltages and taking corresponding images of a moving edge of the mechanism with the microscope system. An image processing program comprised of a simple threshold and line detection algorithm was then applied to the images. The results of five runs of this experiment are shown in Fig. 3. The quadratic behavior is consistent with the actuation physics, where Joule heating caused by voltage-controlled power dissipation across the bent-beam structure results in displacement. The curve fit in Fig. 2 shows that the repeatability in the experiments is reasonable, with a maximum standard deviation of 99 nm at any input voltage value. The camera pixel resolution for the microscope magnification used in the experiments ($\approx 100X$) was 106 nm. Therefore, the repeatability errors are probably partially due to the inherent resolution limitations in optical imaging. However, it is clear that the repeatability error increases for increasing voltage / displacement, indicating that these errors are to some degree physical.

In tandem with the static behavior characterization, the LRM was calibrated by relating the mechanism displacement to the photodiode voltage. First, the optics were aligned to center the beam spot on a moving edge of the mechanism when the mechanism is approximately in the middle of its range. At each input voltage value, the photodiode is measured after taking an image. The relationship between the input voltage and photodiode voltage for a single run of the experiment is shown in Fig. 4. Only one run is shown because we found that there is

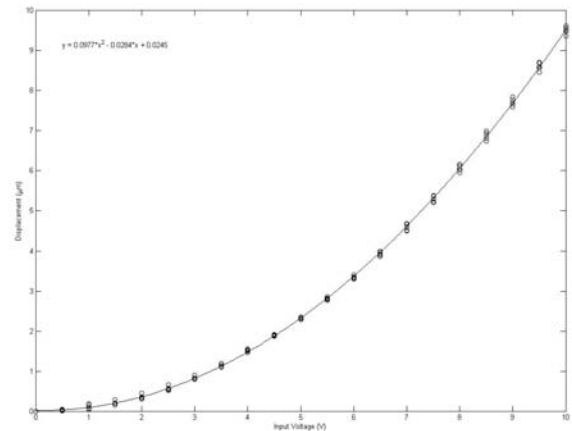


Fig. 3 Measured displacement for varied input voltage

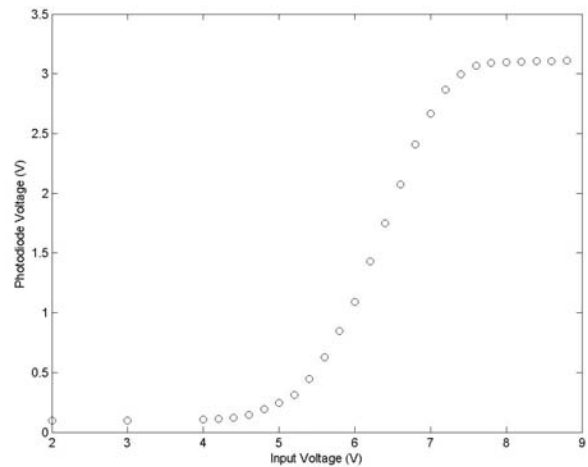


Fig. 4 Measured LRM photodiode voltage for varied input voltage

a systematic drift in this measurement, and there are typically shifts in the data from run to run. However, we found that the drift is slow enough that it has very little effect on a single experiment.

By correlating the displacement measurement obtained from image processing with the photodiode voltages, a calibration curve for the LRM can be determined, as shown in Fig. 5. The data shows that the reflection off of a moving edge as a function of the position is sigmoidal, as would be expected for a Gaussian beam profile. Although there are a number of functions that could be used to fit this data, the following function has been applied due to its simplicity in applying least-squares fitting and inversion:

$$V_{pd} = \frac{A(x - \bar{x})}{((x - \bar{x})^2 + \epsilon^2)^{1/2}} + B \quad (1)$$

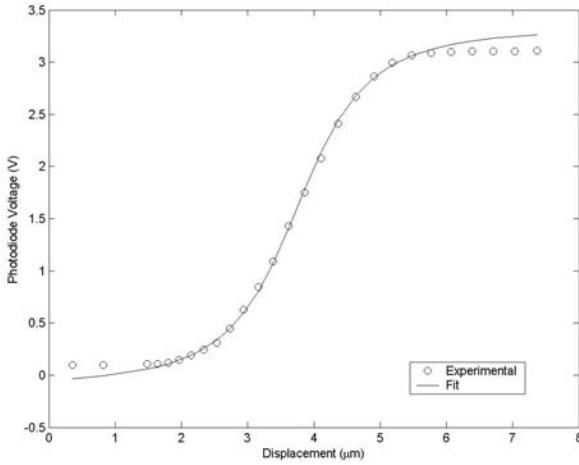


Fig. 5 LRM calibration results (photodiode voltage vs. displacement) with sigmoid fit

where V_{pd} is the photodiode voltage; x is the position of the mechanism; and A , B , \bar{x} , and ε are fit parameters. Figure 5 contains a least-squares fit of the data using this function, with the data points in the center weighted more heavily. The maximum sensitivity was found to be $0.7 \mu\text{m}/\text{V}$, in this case located at $3.8 \mu\text{m}$. The noise from the photodiode at this peak sensitivity has a standard deviation of 3.1 mV , or converting to displacement, 2.17 nm . Therefore, a conservative estimate of the sensing resolution is 5 nm at peak sensitivity. However, this resolution is only valid within a small range. This will be improved considerably in the future by using a higher power laser, thereby minimizing the effects of shot and Johnson noise. Due to the sigmoidal response of the LRM, it is best for measuring small excursions with high resolution such as testing nanopositioning capabilities.

Dynamic Characterization

The bandwidth of the LRM is currently 90 kHz and will likely increase with the addition of a higher power laser, thereby reducing the need for amplification electronics which curtail the sensing bandwidth. Additionally, the LRM output is a low voltage analog signal. Both of these qualities make it particularly suitable for in-plane frequency response measurements of MEMS. This approach has been used to determine the dynamics of the MEMS nanopositioner. A 5 V bias was applied to the mechanism and the beam was centered on a moving edge of the mechanism. Using the swept-sine method on a dynamic signal analyzer, the frequency response was measured as shown in Fig. 6. The dynamics consists of a low-frequency first-order system coupled with a high-frequency lightly-damped second-order system. This is consistent with the mechanism configuration since the thermal actuator is known to have a slow first-order response, while the flexure mechanism is expected to act as a mass-spring-damper system. A model is proposed in the next section that is included in Fig. 6, indicating that the model accurately depicts the linearized system dynamics.

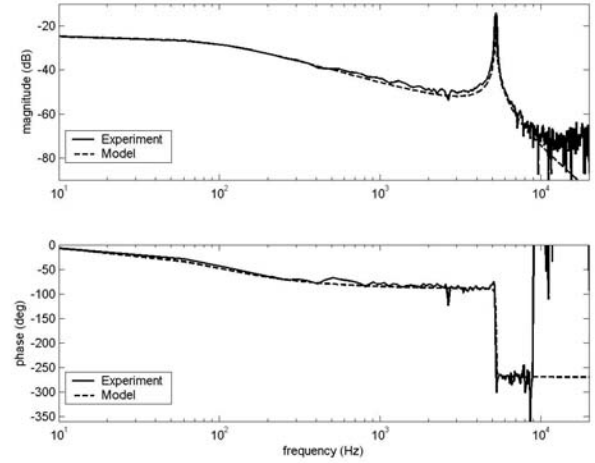


Fig. 6 MEMS nanopositioner experimental frequency response

NANOPositioner MODELING

Based on the static and dynamic characterizations discussed in the previous section, an empirical nonlinear dynamic model has been derived. The model consists of a nonlinear quadratic input model and a third-order linear dynamic model. The nonlinear quadratic model is based on the data presented in Fig. 3 and can be represented as:

$$x_1 = a_2 V^2 + a_1 V + a_0 \quad (2)$$

where x_1 is the mechanism position; V is the input voltage; and the parameters a_0 , a_1 , and a_2 have the values $a_0 = 2.45 \times 10^{-8} \text{ m}$, $a_1 = -2.84 \times 10^{-8} \text{ m/V}$, and $a_2 = 9.77 \times 10^{-8} \text{ m/V}^2$.

The third-order model is comprised of the first-order response of the thermal actuator and the second-order response of the flexure mechanism. The two subsystems can be written in state-space form as:

$$\dot{x}_1 = x_2 \quad (3)$$

$$\dot{x}_2 = -2\xi\omega_n x_2 - \omega_n^2 x_1 + b_1 x_3 \quad (4)$$

$$\dot{x}_3 = -\gamma x_3 + b_2 u(V) \quad (5)$$

The input to the system, $u(V)$, is a nonlinear function of the input voltage that is proportional to Eqn. (2). The static and dynamic models in Eqns. (2-5) should be consistent with the data shown in Figs. 3 and 6, such that the dynamic model provides the same output as the static model for a static input voltage. Examining the steady-state case for the dynamic model by setting $\dot{x}_1, \dot{x}_2, \dot{x}_3 = 0$, it can be found that:

$$x_1 = \frac{b_1 b_2}{\omega_n^2 \gamma} u(V) \quad (6)$$

Comparing this steady-state solution for x_1 with that in Eqn. (2), it is found that:

$$u(V) = \frac{\omega_n^2 \gamma}{b_1 b_2} (a_2 V^2 + a_1 V + a_0) \quad (7)$$

Substituting Eqn. (7) into Eqn. (5), and redefining the control input, the dynamic model (Eqns. (3-5)) can be rewritten as:

$$\dot{x}_1 = x_2 \quad (8)$$

$$\dot{x}_2 = -2\xi\omega_n x_2 - \omega_n^2 x_1 + b_1 x_3 \quad (9)$$

$$\dot{x}_3 = -\gamma x_3 + \frac{1}{b_1} v(V) \quad (10)$$

where:

$$v(V) = \bar{a}_2 V^2 + \bar{a}_1 V + \bar{a}_0 \quad (11)$$

and $\bar{a}_0 = \omega_n^2 \gamma a_0$, $\bar{a}_1 = \omega_n^2 \gamma a_1$, and $\bar{a}_2 = \omega_n^2 \gamma a_2$. The advantage of this representation is that all of the parameters in Eqns. (8-11) can be determined from the experimental results presented in the previous section except for b_1 , which cancels internally, thereby has no effect on the input-output behavior.

The transfer function for the mechanism can be written as:

$$\frac{X_1(s)}{Y(s)} = \frac{1}{(s + \gamma)(s^2 + 2\xi\omega_n s + \omega_n^2)} \quad (12)$$

where $Y(s)$ is the Laplace transform of the nonlinear control input $v(V)$. This transfer function was fit to the experimental frequency response data, as shown in Fig. 6. The natural frequency and damping ratio of the second-order system were found to be $\omega_n = 3.2027 \times 10^4$ rad/s and $\xi = 0.0025$, respectively, and the cutoff frequency of the first-order system is $\gamma = 559.20$ rad/s. The static (Eqn. (2)) and dynamic (Eqns. (8-12)) models are used in the design and implementation of several control system approaches for the MEMS nanopositioner in the following section.

CONTROL APPROACHES

The precision motion control of MEMS has received only limited attention in the literature, partially because many MEMS do not require high levels of precision. Some of the critical issues in designing a MEMS precision motion controller, including performance tradeoffs, the benefits of open-loop control and closed-loop control, and sensing issues have previously been investigated [9-11]. However, the particular question of which control approach is best when nano-scale precision is required has not been answered. In this section, three classical control approaches, quasi-static nonlinear open-loop control, nonlinear forward compensation,

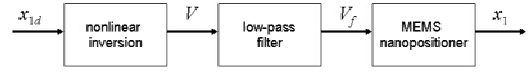


Fig. 7 Quasi-static open-loop controller

and nonlinear PI control, are used to design appropriate controllers for the MEMS nanopositioner. Simulation results for each of these controllers are used to explore the limitations of each approach with regard to the desired nano-scale performance.

Quasi-Static Open-Loop Control

Open-loop control is probably the most common approach for MEMS because: 1) it does not require sensor feedback, simplifying the design, reducing the footprint of the device, and eliminating the need for on-chip signal conditioning; and 2) can be implemented on many devices simultaneously without the need for high performance control electronics. Many MEMS actuators, including thermal, electrostatic and magnetic, are inherently stable in that a constant input voltage, or current, results in a constant displacement. The simplest open-loop controller that can achieve some level of positioning precision is a quasi-static controller based on the static relationship between the input voltage and the resulting displacement.

The quasi-static nonlinear controller is designed by solving for the input voltage, V , in Eqn. (2), and choosing the positive valued solution such that:

$$V = \frac{-a_{1c} + (a_{1c}^2 - 4a_{2c}(a_{0c} - x_{1d}))^{1/2}}{2a_{2c}} \quad (13)$$

where x_{1d} is the desired position, and a_{0c} , a_{1c} , and a_{2c} are the controller parameters which are the measured values discussed previously. The accuracy between these parameters and the mechanism's actual parameters a_0 , a_1 , and a_2 will determine the accuracy at which the MEMS can quasi-statically position using this controller.

The block diagram for the controller is shown in Fig. 7. A desired position, x_{1d} , is used to calculate an input voltage using Eqn. (13). The input voltage is then passed through a first-order low-pass filter with a cutoff frequency of $\omega_f = 3.142 \times 10^3$ rad/s to minimize excitation of the system's resonance, before being applied directly to the mechanism. A simulation of the controller has been implemented in Matlab and Simulink, using the nonlinear third-order model for the MEMS nanopositioner (Eqns. (8-11)).

The effects of uncertainty in the model parameters a_0 , a_1 , and a_2 when tracking a sinusoidal position have been studied. In Fig. 8, the variations in tracking performance for a 2 Hz 1 μm amplitude signal are shown when all three model parameters go from -5 % to +5 % of their nominal values. Obviously, when the model and controller have the same parameters, the tracking performance is excellent for this low-bandwidth signal. However, the effects of uncertainty in this

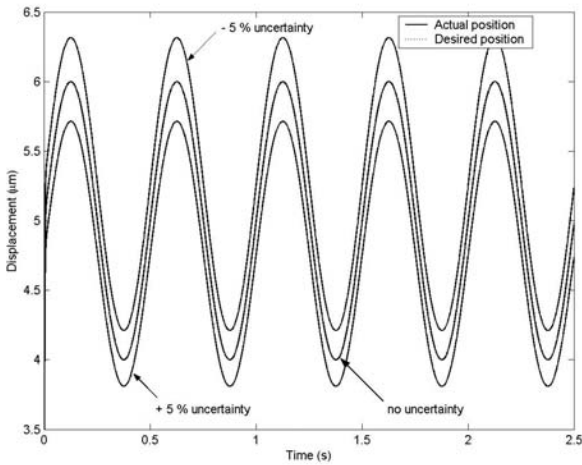


Fig. 8 Tracking 1 μm amplitude sinusoid with open-loop controller

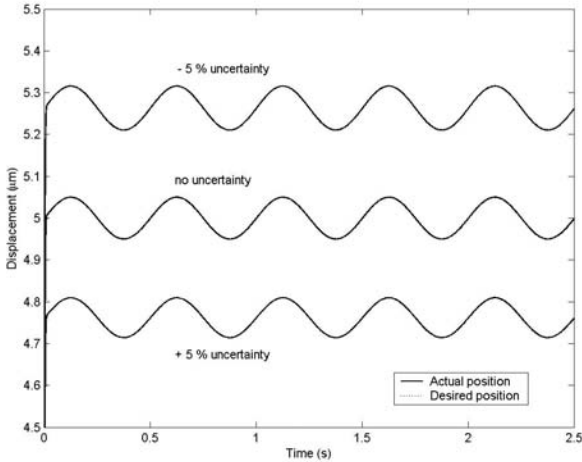


Fig. 9 Tracking 50 nm amplitude sinusoid with open-loop controller

case are extreme. Within this range of uncertainty, the position errors are ± 53 nm in amplitude and ± 293 nm in the DC offset. Similar results were found when tracking a 50 nm amplitude position trajectory, as shown in Fig. 9.

Based on these results, it is clear that very small uncertainties in the model will cause severe limitations in nanopositioning accuracy. Therefore, it is critical that the model parameter measurements are shown to be repeatable. Furthermore, environmental conditions would have to be controlled for this approach to work since the model parameters will change as a function of temperature in the working environment.

Forward Compensation

In addition to the problems with robustness discussed above, the quasi-static open-loop controller is limited by the open-loop bandwidth of the thermal actuator, which is approximately 89 Hz. There are a number of methods for

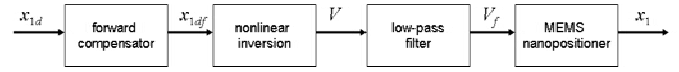


Fig. 10 Forward compensation controller

increasing the bandwidth using an open-loop controller including the input shaping approaches discussed in [9,10]. Due to its simplicity, forward compensation is utilized here. The objective of the design is to cancel the pole in the thermal actuator dynamics, represented by γ in Eqns. (8-11), and replace it with a fast pole to decrease the system's rise time. Additionally, the forward compensator should have a unity DC gain. The forward compensator used here is:

$$\frac{X_{1df}(s)}{X_{1d}(s)} = \rho \frac{s + \gamma_c}{s + \gamma_*} \quad (14)$$

where γ_c is equal to γ when there is no model uncertainty, γ_* is the faster pole to be inserted into the dynamics, and $\rho = \gamma_*/\gamma_c$.

The forward compensator is added to the input side of the control path, as shown in Fig. 10. Simulations have been used to study the forward compensator's effect on the system's rise time. First, a square wave with an amplitude of 1 μm , a frequency of 50 Hz, and a DC offset of 5 μm , was applied and γ_* was varied between one (no FC), two (2X FC) and three (3X FC) times γ_c . In Fig. 11, the response for each of these values is shown, indicating a dramatic improvement in the rise time using the forward compensator. Without the compensator, the rise-time is 4.2 ms, while with the compensator, the rise time was decreased to 2.2 ms when $\gamma_* = 2\gamma_c$, and 1.5 ms for $\gamma_* = 3\gamma_c$. However, the reduction in rise-time increased the amplitude of nano-scale resonant vibrations, which could be an issue in some applications.

Another problem caused by this approach is a large control effort, particularly when $\gamma_* = 3\gamma_c$, as shown in Fig. 12. The control voltage ranges from 0.8 V to 10.2 V. This is a somewhat expected problem but the allowable voltage range for the MEMS nanopositioner, and many other MEMS, makes this particularly problematic. A spike in voltage can easily destroy a thermal actuator. The actuators studied in this paper typically break between 14 V and 18 V. Additionally, negative voltage results in the same displacement as a positive voltage with the same value. Therefore, if the spike goes negative, the controller will generate an undesirable motion. As shown in Figs. 13 and 14, the control voltages are far more reasonable when tracking a 50 nm square wave. This indicates that forward compensation may be best for decreasing rise time only when tracking small signals and while within the middle of the mechanism's motion range.

PI Control

Closed-loop control is the obvious answer to the robustness issues associated with the previously discussed open-loop

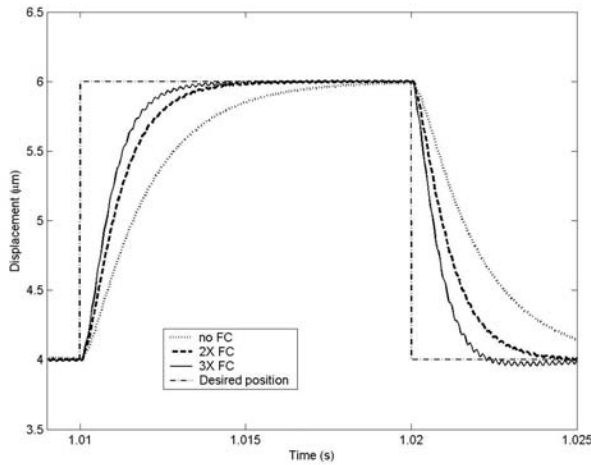


Fig. 11 Tracking 1 μm amplitude square wave with forward compensation

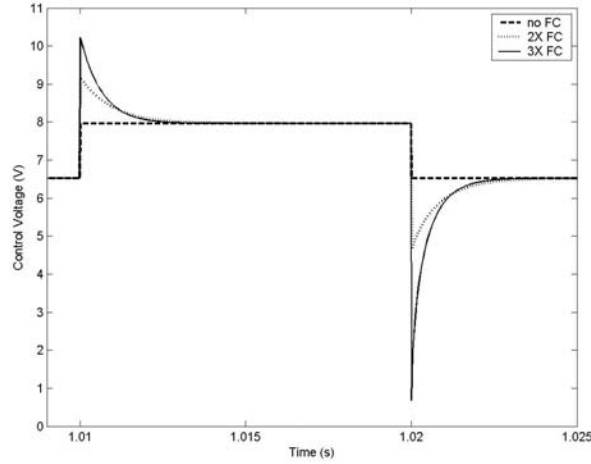


Fig. 12 Control effort when tracking 1 μm amplitude square wave with forward compensation

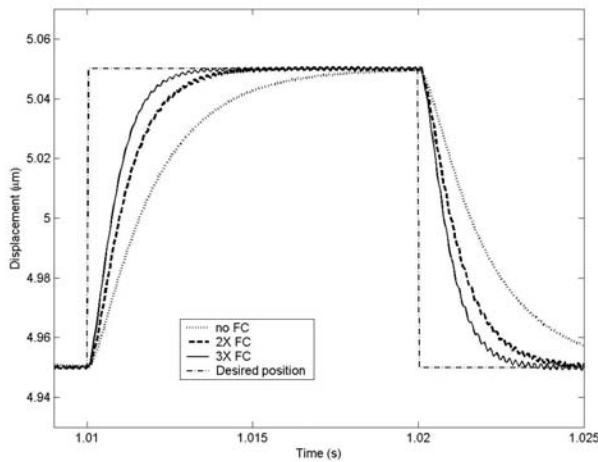


Fig. 13 Tracking 50 nm amplitude square wave with forward compensation

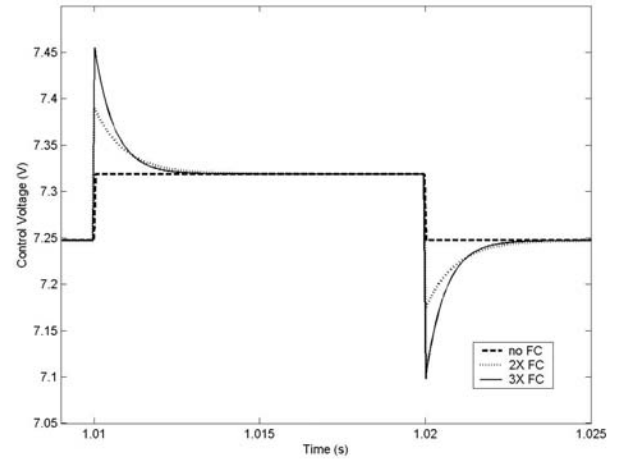


Fig. 14 Control effort when tracking 50 nm amplitude square wave with forward compensation

approaches. In order to deal with the nonlinear behavior of the mechanism and improve both robustness and bandwidth, a controller has been designed that combines a standard PI controller with the nonlinear inversion approach previously discussed, as described in Fig. 15. The low-pass filter remains in the feedback loop to minimize excitation of the structural resonance. The PI controller is in the standard form:

$$\frac{Y(s)}{E(s)} = \frac{K_p s + K_i}{s} \quad (15)$$

where $Y(s)$ is the Laplace transform of the nonlinear control input v , and the nonlinear inversion function is:

$$V = \frac{-\bar{a}_{1c} + \left(\bar{a}_{1c}^2 - 4\bar{a}_{2c}(\bar{a}_{0c} - v)\right)^{1/2}}{2\bar{a}_{2c}} \quad (16)$$

The parameters \bar{a}_{0c} , \bar{a}_{1c} , and \bar{a}_{2c} are the measured values of \bar{a}_0 , \bar{a}_1 , and \bar{a}_2 . These parameters are used instead of a_0 , a_1 , and a_2 because the nonlinear portion of the controller is designed to linearize the control input but is not intended to provide the appropriate DC gain to achieve the desired position.

Similar to the previous two controllers, this approach was simulated with the nonlinear third-order model. The PI controller gains were designed to make the closed-loop system critically damped and have a natural frequency of 628.3 rad/s. In this case, the rise time was found to be 1.9 ms. Similar to the open-loop approach, robustness to variations in the quadratic model was investigated by varying these parameters by $\pm 5\%$. The response of the system for this parameter range is shown in Fig. 16. It is clear that the parameter variations have very little effect on the system's performance. The control effort was also smaller for the nonlinear PI controller compared to the forward compensator for equivalent rise time, as shown in Fig. 17.

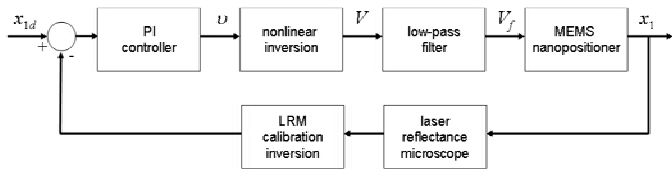


Fig. 15 PI controller with nonlinear inversion and LRM calibration

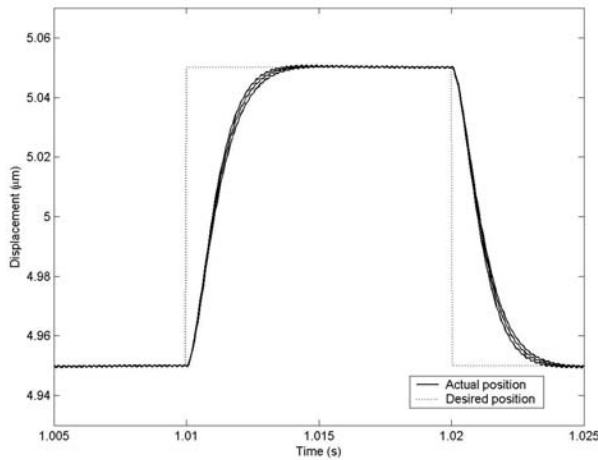


Fig. 16 Tracking 50 nm amplitude square wave with PI control

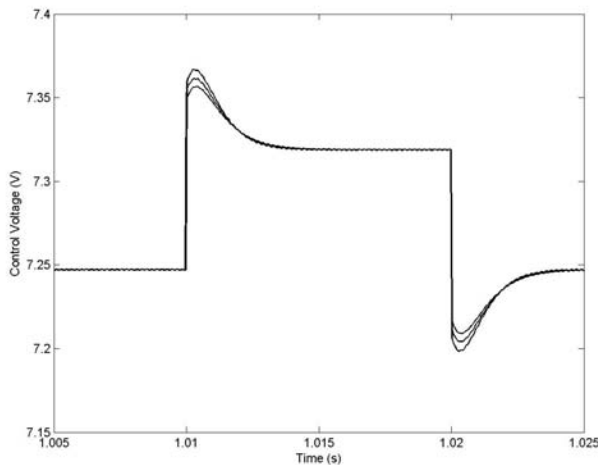


Fig. 17 Control effort when tracking 50 nm amplitude square wave with PI control

Based on these results, it is clear that the nonlinear PI controller provides the best results in terms of increased bandwidth, tracking accuracy, robustness and control effort. This is an expected result but the degree to which it is true is important in selecting a controller for MEMS nanopositioner applications. Forward compensation can increase bandwidth but causes positioning inaccuracies by exciting resonant vibrations. Uncertainty in the quadratic response of the thermal

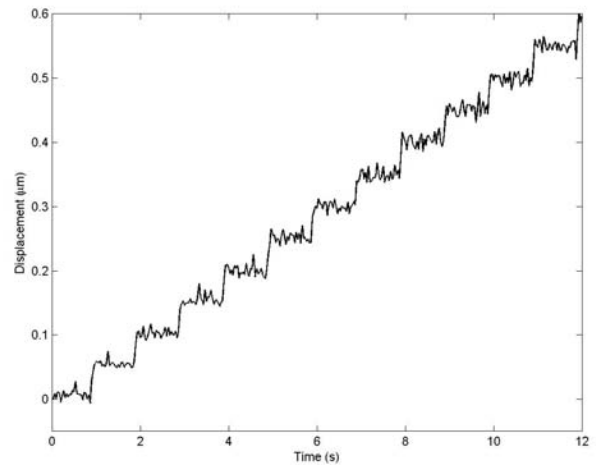


Fig. 18 Tracking 50 nm steps with open-loop control

actuator also results in inaccuracies that are unacceptable in most applications. The exception are those applications which do not require enhanced bandwidth and can provide a controlled environment in which the thermal actuator behavior can be measured with extremely high accuracy. Even in these cases, errors are likely to result, as discussed in the next section. Therefore, closed-loop control is necessary for nano-scale positioning resolution and the proposed nonlinear PI controller is a reasonable baseline solution for this problem.

EXPERIMENTAL RESULTS

The first open-loop control approach discussed in the previous section was implemented on a MEMS nanopositioner using calibration data similar to that shown in Fig. 3. In this case, the mechanism was operated in a scanning electron microscope (SEM), and the positioning accuracy and resolution were measured by applying image processing to the SEM video signal, which in this case had a pixel resolution of 4.4 nm. The controller was used to generate 50 nm steps, as shown in Fig. 18. The position resolution was found to be below 12 nm and the step repeatability was ± 7 nm. Although these results indicate that the controller is capable of nano-scale resolution, we found that for larger steps, the accuracy decreases significantly as predicted by the simulation results from the previous section.

CONCLUSION

Three classical control approaches for controlling a MEMS nanopositioner were analyzed and simulation results were presented that indicate that closed-loop control is in general a prerequisite to achieve nano-scale positioning resolution with robustness. The first approach is a quasi-static open-loop controller which inverts a quadratic function relating the input voltage to the resulting displacement, thereby calculating a control voltage given a desired position. This approach was then improved by adding a forward compensator to decrease the rise time of the system. The final approach merges the inversion of the quadratic function with a PI controller. Using simulations based on experimental static and dynamic

characterization results for the mechanism, each control approach was evaluated. Small amounts of uncertainty in the open-loop control design were shown to result in positioning accuracies that are unacceptable for most nanopositioning applications. The nonlinear PI controller was shown to increase the bandwidth, achieve nano-scale positioning resolution and demonstrated reasonable robustness. This approach will be implemented experimentally on the MEMS nanopositioner in the near future.

REFERENCES

- [1] Xu, Y., MacDonald, N. C., and Miller, S. A., 1995, "Integrated micro-scanning tunneling microscope," *Applied Physics Letters*, **67**, pp. 2305-2307.
- [2] Eleftheriou, E. et al., 2003, "Millipede - A MEMS-based scanning-probe data-storage system," *IEEE Transactions on Magnetics*, **39**, pp. 938-945.
- [3] Gollasch, C. O., Mektadir, Z., Kraft, M., Trupke, M., Eriksson, S., and Hinds, E. A., 2005, "A three-dimensional electrostatic actuator with a locking mechanism for microcavities on atom chips," *Journal of Micromechanics and Microengineering*, **15**, pp. S39-S46, 2005.
- [4] Horsley, D. A., Wongkomet, N., Horowitz, R., and Pisano, A. P., 1999, "Precision positioning using a microfabricated electrostatic actuator," *IEEE Transactions on Magnetics*, **35**, pp. 993-999.
- [5] Hoen, S. et al., 2003, "A high-performance dipole surface drive for large travel and force," *Proceedings of Transducers '03*, Boston, MA, pp. 344-347.
- [6] Hubbard, N. B. and Howell, L. L., 2005, "Design and characterization of a dual-stage, thermally actuated nanopositioner," *Journal of Micromechanics and Microengineering*, **15**, pp. 1482-1493.
- [7] Bergna, S., Gorman, J. J., and Dagalakis, N. G., 2005, "Design and modeling of thermally actuated MEMS nanopositioners," *Proceedings of the ASME IMECE*, Orlando, FL, IMECE2005-82158.
- [8] Hickey, R., Sameoto, D., Hubbard, T., and Kujath, M., 2003, "Time and frequency response of two-arm micromachined thermal actuators," *Journal of Micromechanics and Microengineering*, **12**, pp. 40-46.
- [9] Popa, D. O., Kang, B. H., Wen, J. T., Stephanou, H. E., Skidmore, G., and Geisberger, A., 2003, "Dynamic modeling and input shaping thermal bimorph MEMS actuators," *Proceedings of the IEEE International Conference on Robotics and Automation*, Taipei, Taiwan, pp. 1470-1475.
- [10] Borovic, B., Liu, A. Q., Popa, D., Cai, H., and Lewis, F. L., 2005, "Open-loop versus closed-loop control of MEMS devices: choices and issues," *Journal of Micromechanics and Microengineering*, **15**, pp. 1917-1924.
- [11] Messenger, R. K., McLain, T. W., Howell, L. L., 2004, "Feedback control of thermomechanical inplane microactuator using piezoresistive displacement sensing," *Proceedings of the ASME IMECE*, Anaheim, CA, IMECE2004-59810.